PHYSICAL REVIEW C VOLUME 18, NUMBER 5 NOVEMBER 1978

Cross-section measurements and phase shift analysis of p-^{4}He elastic scattering in the energy range 20–55 MeV*

A. Houdayer
Cyclotron Laboratory, Department of Physics, University of Manitoba, Winnipeg, Manitoba R3T 2N2, Canada and Foster Radiation Laboratory, McGill University, Montreal, Quebec H3C 3G1, Canada

N. E. Davison, S. A. Elbakr,† A. M. Sourkes,‡ and W. T. H. van Oers
Cyclotron Laboratory, Department of Physics, University of Manitoba, Winnipeg, Manitoba R3T 2N2, Canada

A. D. Bacher
Department of Physics, Indiana University, Bloomington, Indiana 47401
(Received 23 May 1978)

Measurements have been made of the $p + {}^4$He elastic scattering angular distributions at $T = 21.85$, 23.90, 25.75, 28.10, 30.35, 32.15, 34.25, 36.90, 39.75, 42.45, 44.05, 44.95, and 47.65 MeV in the angular range $10° \lesssim \theta_{c.m.} \lesssim 170°$. The data obtained have in general relative errors smaller than 2%, while the absolute scale of the measurements has an uncertainty of less than 2.5%. These data together with differential cross sections and analyzing power angular distributions selected from the literature, as well as total reaction cross section information have been subjected to a phase shift analysis. Up to 45 MeV a single, continuous solution could be determined using phase shifts up through G-waves. As in an earlier phase shift analysis the phase shifts exhibit a smooth variation with energy except for the well-known resonance region around 23.4 MeV. Above 45 MeV some improvement was obtained with the inclusion of a small H-wave contribution. New total reaction cross section data were employed as a constraint on the imaginary parts of the phase shifts. The new analysis corroborates an early finding that the inelasticity is mainly associated with the even partial waves.

[NUCLEAR REACTIONS Measured $d\sigma/d\Omega$ for ^{4}He$(p,p)^4$He at $T = 21.85$, 23.90, 25.75, 28.10, 30.35, 32.15, 34.25, 36.90, 39.75, 42.45, 44.05, 44.95, and 47.65 MeV for $10° \lesssim \theta_{c.m.} \lesssim 170°$; phase shift analysis using $d\sigma/d\Omega$ and other selected $d\sigma/d\Omega$, A, and σ_R from the literature, 20 MeV $< T \leq 55$ MeV.]

INTRODUCTION

The elastic scattering of protons from ^{4}He is one of the simpler systems amenable to a phase shift analysis aiding in the theoretical interpretation of the few-nucleon system ^{5}Li. Over the years there has been a continual improvement in the quality of the experimental data, be it differential cross sections, analyzing powers, or total reaction cross sections, in the precision with which the phenomenological analyses fit the experimental data, and in the theoretical representations of this five-nucleon system. There is reason to accept that once the phase shifts obtained in single energy analyses exhibit a continuous behavior as a function of energy starting at zero energy a unique solution has been obtained.

Recently Plattner *et al.*[1] presented a phase shift analysis of $p + {}^4$He elastic scattering in the energy range 20–40 MeV. The data analyzed included both polarizations and differential cross sections.[2] The errors associated with the differential cross section data were significantly larger than those of the polarization data mainly as a result of the method of normalization adopted. In addition, there was a lack of reaction cross-section information, thus precluding direct constraints on the inelastic parameters. In order to improve on the accuracy of the existing data set, the present measurements of $p + {}^4$He elastic scattering differential cross sections angular distributions were made, where possible, at the same energies as the polarization angular distributions of Bacher *et al.*[2] In a separate experiment measurements were also made of the $p + {}^4$He total reaction cross sections from threshold near 23 to 48 MeV.[3] After augmenting the data set at the higher energies with a few selected angular distributions from the literature, a phase shift analysis was made for the energy range from 20 to 55 MeV.

Phase shift analyses for the energy region below 20 MeV are numerous (Refs. 4–8, and references therein) and provide a reasonably similar description of the quite precise data that has been accumulated for that energy region. There is some evidence that of the earlier analyses the one of

 © 1978 The American Physical Society

TABLE I. Gas scattering geometry.

Detector	R (cm)	h (cm)	$2a$ [a] (cm)	l [a] (cm)	$2b$ (cm)	G_∞ (10^{-4} cm)	$\Delta G_\infty/G_\infty$ (%)
			$T_p < 39.75$ MeV				
0	33.223	27.747	0.1554	0.3115	0.475	0.2423	1.80
1	33.228	27.755	0.3213	0.6331	0.475	1.0204	0.70
2	33.228	27.757	0.3184	1.267	0.475	2.0496	0.56
3	33.231	27.755	0.3150	1.263	0.475	2.0204	0.94
4	33.223	27.747	0.3171	1.267	0.475	2.0427	1.00
5	33.231	27.752	0.3168	1.268	0.475	2.0412	0.72
6	33.228	27.750	0.3189	1.264	0.475	2.0495	1.11
7	33.221	27.742	0.3169	1.265	0.475	2.0389	0.66
			$T_p \geq 39.75$ MeV				
0	33.233	27.803	0.3144	0.6305	0.476	0.9943	0.62
1	33.226	27.795	0.4805	1.276	0.476	3.1343	0.59
2	33.231	27.800	0.4734	1.266	0.476	3.0622	0.58
3	33.226	27.795	0.4752	1.265	0.476	3.0733	0.58
4	33.223	27.793	0.4786	1.271	0.476	3.1103	0.58
5	33.221	27.790	0.4725	1.265	0.476	3.0564	0.59
6	33.218	27.788	0.4762	1.267	0.476	3.0845	0.59
7	33.213	27.783	0.4834	1.273	0.476	3.1496	0.58

[a] Note that the solid angle defining apertures had rounded-off corners.

Arndt *et al.*[6] provides a better description of very recently measured $p-{}^4$He observables for the energy region 2.2 to 8.9 MeV.[9] The most elaborate R-matrix analysis for the energy region 0 to 18 MeV (Ref. 8) included all available differential cross section and spin-dependent observables that passed rather strict statistical criteria. Above 20 MeV the phase shift solution of Plattner *et al.*[1] matches smoothly with the energy-dependent phase shifts derived by Schwandt *et al.*[5] The set of phase shifts obtained by Plattner *et al.* showed that the inelasticity occurs predominantly in the even partial waves. There was only weak evidence in the energy dependence of the phase shifts for structure

TABLE II. Contributions to the relative uncertainties in the differential cross sections.

Type of uncertainty	$T_p < 39.75$ MeV	$T_p \geq 39.75$ MeV
Counting statistics	<1%	<1.7%
Deadtime correction	±20% of the correction	±20% of the correction
Subtraction of contaminants yields	...	±20% of the correction
Integration of the beam current (relative)	±0.5%	±0.5%
Geometry factor	See Table I	See Table I
Detector angle (relative)	±0.03°	±0.03°
Pressure	±2.5 Torr	±2.5 Torr
Temperature	±0.5°	±0.5°
Finite geometry correction	±0.1%	±0.1%

TABLE III. Contributions to the uncertainty in the absolute scale of the differential cross sections.

Type of uncertainty	
Detector angle (absolute)	±0.1°
Reproducibility of the measurements	±1.3%
Energy of the incident proton beam	±0.4%
Energy-degraded proton contamination	<0.1%
Correction for reactions in the NaI(Tl) detectors	±15% of the correction

in ^{5}Li other than the well known $3/2^+$ second excited state at 16.7 MeV. With the exception of the $^2D_{3/2}$ real phase shift and inelastic parameter, all other phase shifts showed a rather slow variation with energy. The present analysis was made in order to give some of these results a more quantitative basis and to investigate the behavior of the phase shifts towards higher incident proton energies. As a practical application, values of the analyzing power may be determined from such an analysis that will be useful for the calibration of polarimeters.

EXPERIMENTAL ARRANGEMENTS

The experiment was performed using the external proton beam facility of the University of Manitoba sector-focused cyclotron. The energy of the proton beam was determined by a 45° deflection through a calibrated bending magnet. The calibration of the bending magnet was checked by crossover measurements[10] using a CD_2 target at nominal energies of 23.25, 33.70, and 45.00 MeV and by an observation of the well known $J^\pi = 3/2^+$ resonance in ^{5}Li at an excitation energy of 16.68 MeV (corresponding to an incident proton energy of 23.39 MeV).[11,12] From this and previous measurements the calibration of the bending magnet was found to be accurate to ±0.2% in the momentum.

The scattering chamber (115 cm internal diam-

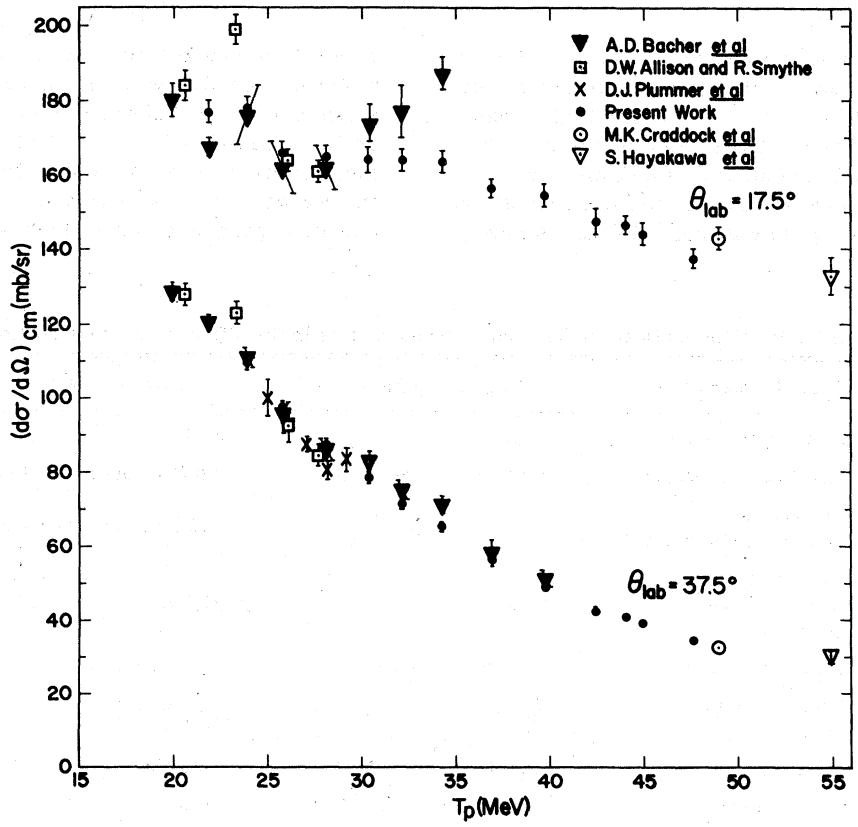

FIG. 1. Excitation functions for ^{4}He$(p,p)^4$He elastic scattering in the energy range 20 to 55 MeV for laboratory scattering angles $\theta_{lab} = 17.5°$ and $\theta_{lab} = 37.5°$.

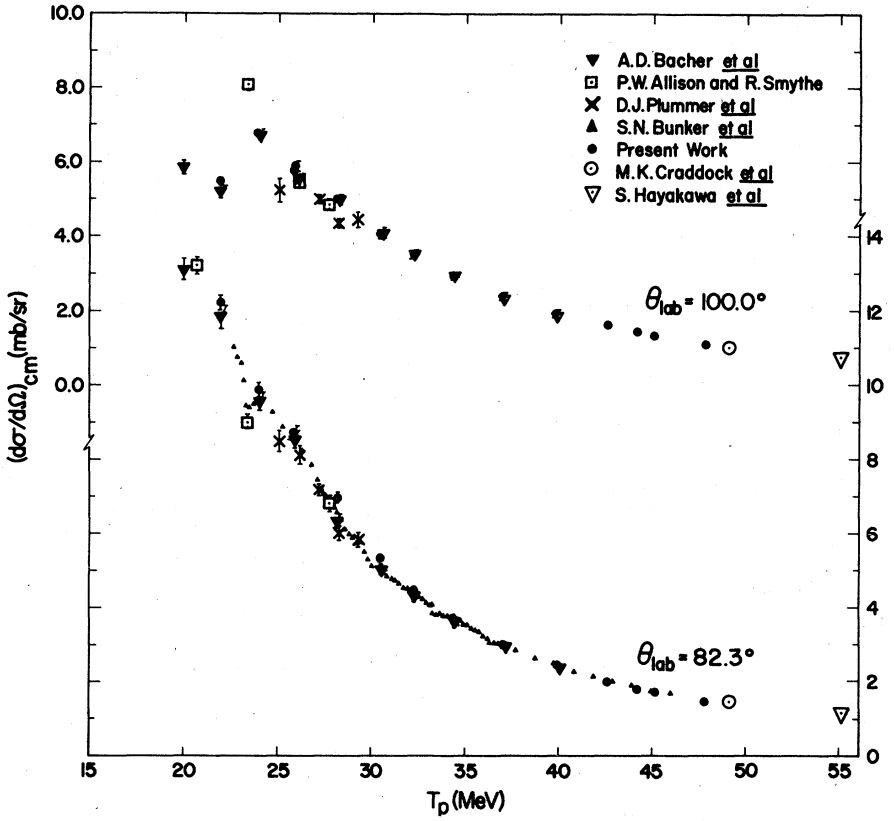

FIG. 2. Excitation functions for $^4He(p,p)^4He$ elastic scattering in the energy range 20 to 55 MeV for laboratory scattering angles $\theta_{lab} = 100.0°$ and $\theta_{lab} = 82.3°$.

eter) contained an array of eight NaI(Tl) scintillation detectors coupled to RCA 4523 photomultiplier tubes which were placed inside a sector shaped box isolated from the vacuum in the scattering chamber by 76 μm thick Kapton-H foil windows. The NaI(Tl) crystals (1.25 cm thick, 3.76 cm diameter) were covered with 25 μm thick aluminum. The sector shaped box held eight solid angle defining collimators made of 0.40 cm copper with accurately machined apertures positioned at a radius of 33.226 cm with respect to the scattering chamber center. The separation between the apertures was $10.00° \pm 0.01°$. The detector box was placed on a turntable and could be set remotely with an accuracy of $\pm 0.02°$. The requirements of a gas scattering geometry were met by a cylindrical collimator containing eight target thickness defining slots with a width of 0.475 cm cut at intervals of $10.00° \pm 0.01°$. The cylindrical collimator (brass 0.429 cm thick) was positioned at a radius of 5.476 cm with respect to the scattering chamber center and was followed by two sets of antiscattering baffles. The scattering chamber and detection apparatus were aligned optically using a theodolite. The distances of the various collimators with respect to the scattering chamber center were measured with precision calipers while the apertures of the collimators were measured with a travelling microscope. The geometry used is given in Table I using the notation of Silverstein.[13]

The ^4He target gas (99.999% purity) was contained in a 8.6 cm diameter gas cell which had a 50 μm thick Kapton-H foil window 1.60 cm high extending over 360° with the exception of two support posts 30° wide. The gas cell was connected to a buffer volume which allowed a constant pressure to be maintained despite the permeability of Kapton-H foil. Before filling the target volume the ^4He gas was cleansed by being passed through a liquid-nitrogen trap. The gas pressure was determined at the beginning and at the end of each experimental run using a precision mechanical absolute pressure gauge calibrated to an accuracy of ± 2.5 Torr. Standard data taking conditions were with a pressure of 1000 Torr. Continuous monitoring of the gas pressure was possible using closed circuit television. The calibration of the pressure

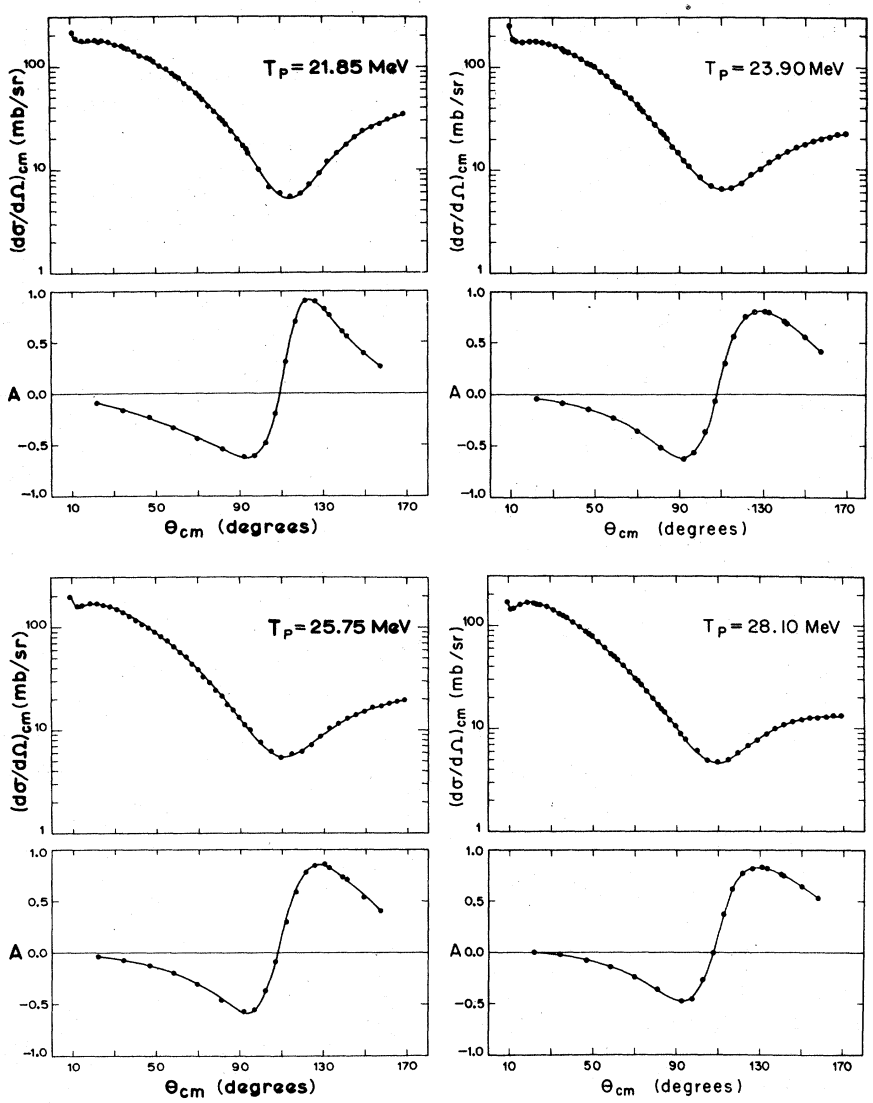

FIG. 3. Differential cross sections at 21.85, 23.90, 25.75, and 28.10 MeV measured in the present experiment and analyzing powers of Bacher *et al*. The solid curves represent the results of the present phase shift analysis.

gauge was checked against a number of other precision pressure gauges. The temperature of the target gas was monitored continuously by measuring the resistance of a calibrated semiconductor thermister exposed directly to the gas in the cell. The temperature could be measured with an accuracy of 0.5°.

The proton beam traversing the target cell was captured in a well-shielded 1.75 m long Faraday cup lined with 2.5 cm thick graphite. The vacuum in the Faraday cup was separated from the vacuum in the scattering chamber by two 75 μm thick Kapton-H foils and 2.5 cm of air. An electron suppression ring prevented electrons including δ rays from entering or leaving the charge collecting part of the Faraday cup. The proton beam charge was integrated using a standard current indicator-integrator with an absolute digitizing accuracy of 0.05%.

The electronic instrumentation consisted of standard slow linear electronic modules (charge sensitive preamplifiers, linear amplifiers, timing single channel analyzers, linear gates and stretchers, summing amplifiers, four analog to digital converters (ADC's), and an online computer). The detectors were arranged in four pairs. The pulses from each member of a pair were tagged and then fed into a common ADC. The output of each single channel analyzer was scaled and divided by the sum of counts in the corresponding spectrum

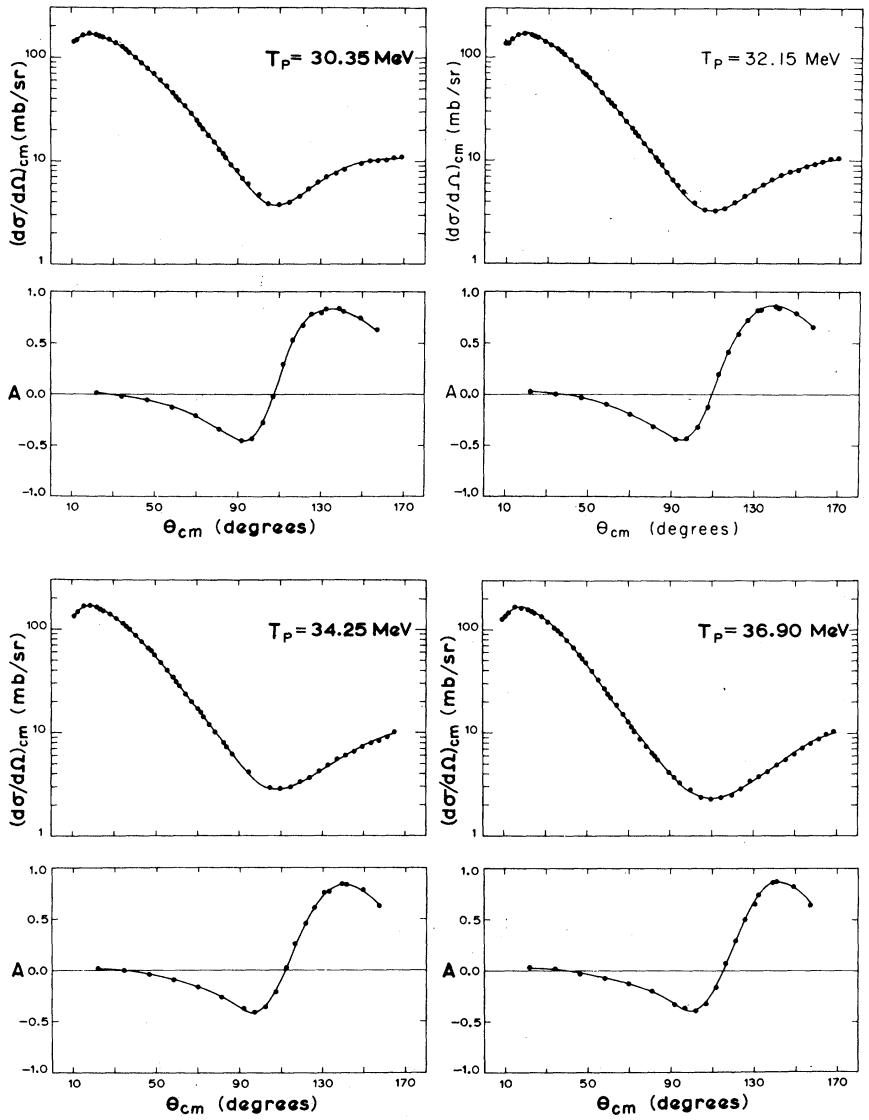

FIG. 4. Differential cross sections at 30.35, 32.15, 34.25, and 36.90 MeV measured in the present experiment and analyzing powers of Bacher *et al.* The solid curves represent the results of the present phase shift analysis.

stored in the computer to give a correction factor for the ADC deadtime. Attached to the scattering chamber were two monitor detectors [NaI(Tl) scintillators] positioned at equal angles (15.0°) to the left and right with respect to the zero degree axis of the scattering chamber. The two monitor detectors had closely similar solid angles.

EXPERIMENTAL PROCEDURES

Before measurements were initiated at each energy, a waist of the incident beam was carefully positioned at the center of the scattering chamber. After passing through the momentum analysis slits at the focal plane of the 45° bending magnet, no further beam defining collimators were employed. Thus it was necessary to determine that the direction of the incident beam coincided with the zero degree axis of the scattering chamber. This was accomplished using the two monitor counters viewing a thin nickel foil. It was required that the ratio of the yields of elastically scattered protons be equal to 1.00 ± 0.02. Slight adjustments in the beam transport parameters were made until this condition was met. The check was repeated regularly between data taking runs. Only occasionally was it necessary to make adjustments to the beam transport parameters after the initial alignment had been carried out. A typical beamspot at the scattering chamber center was

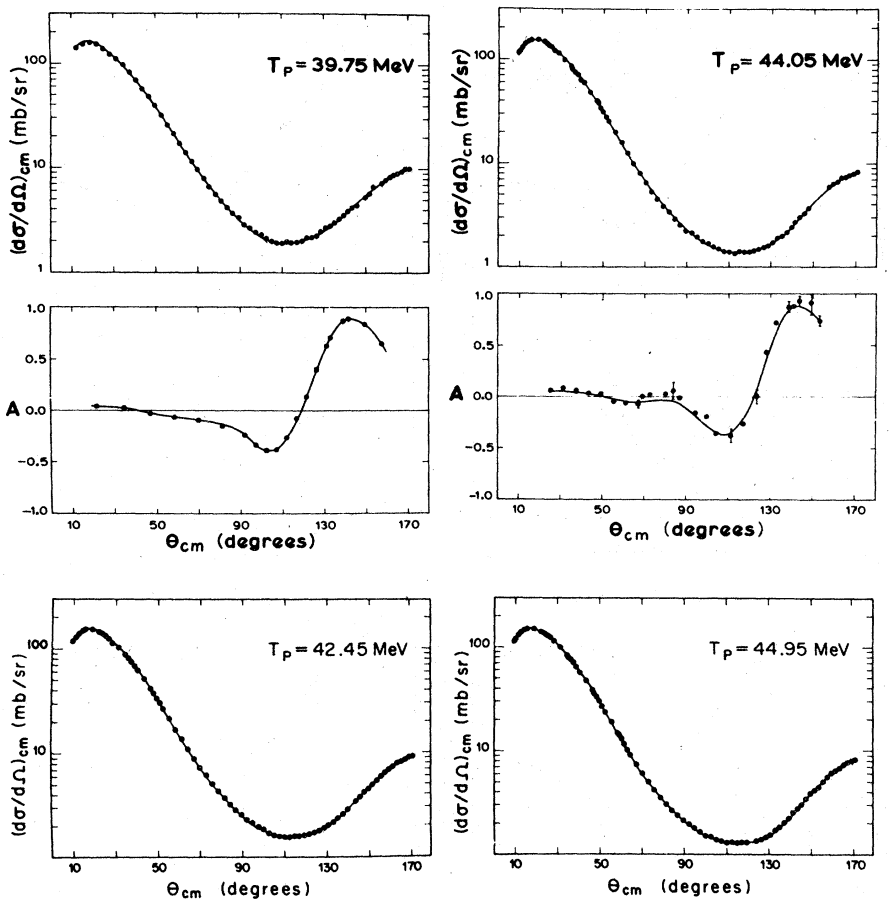

FIG. 5. Differential cross sections at 39.75, 42.45, 44.05, and 44.95 MeV measured in the present experiment and analyzing powers of Bacher *et al.* (39.8 MeV) and Boschitz *et al.* (44.1 MeV). The solid curves represent the results of the present phase shift analysis.

0.3 cm wide by 0.8 cm high with a horizontal angular divergence of less than 22 mrad.

The beam currents on target were about 20 nA except during measurements at extreme forward angles when the beam current was reduced to keep the ADC deadtime correction less than 5%. The energy spread of the incident beam was estimated to be 150 keV [full width at half maximum (FWHM)].

Data were taken at eight angles simultaneously. Thus only a limited number of angular settings were required. At energies equal to or greater than 39.75 MeV, angular distributions were measured in steps of 2.5° between 10° and 170° in the laboratory. The angular distributions were measured with the detector array on one side on the incident beam direction except for occasional checks with the detector array on the opposite side of the incident beam direction to see if the measured differential cross sections agreed within their respective errors. From these checks and from the small drifts in the ratio of the yields of the monitor detectors (within the allowed limits), it was deduced that at all times the incident beam direction coincided with the zero degree axis of the scattering chamber to within 0.05°. To be conservative, the error in the angular scale of the differential cross section angular distributions was taken to be ±0.1°. At energies below 39.75 MeV the data at forward angles ($\theta_{lab} < 60°$) and backward angles ($\theta_{lab} > 120°$) were the averages of measurements left and right with respect to the incident beam direction. The angular distributions at these energies were measured in steps of 2.5° at angles forward of 80° and in steps of 5° for the larger angles.

Since there was no collimation of the incident beam in front of the scattering chamber, checks were made on the extent of possible low intensity wings to the main beamspot. It was found that more than 99% of the incident beam passed through a circular area with a diameter of 1.5 cm at the

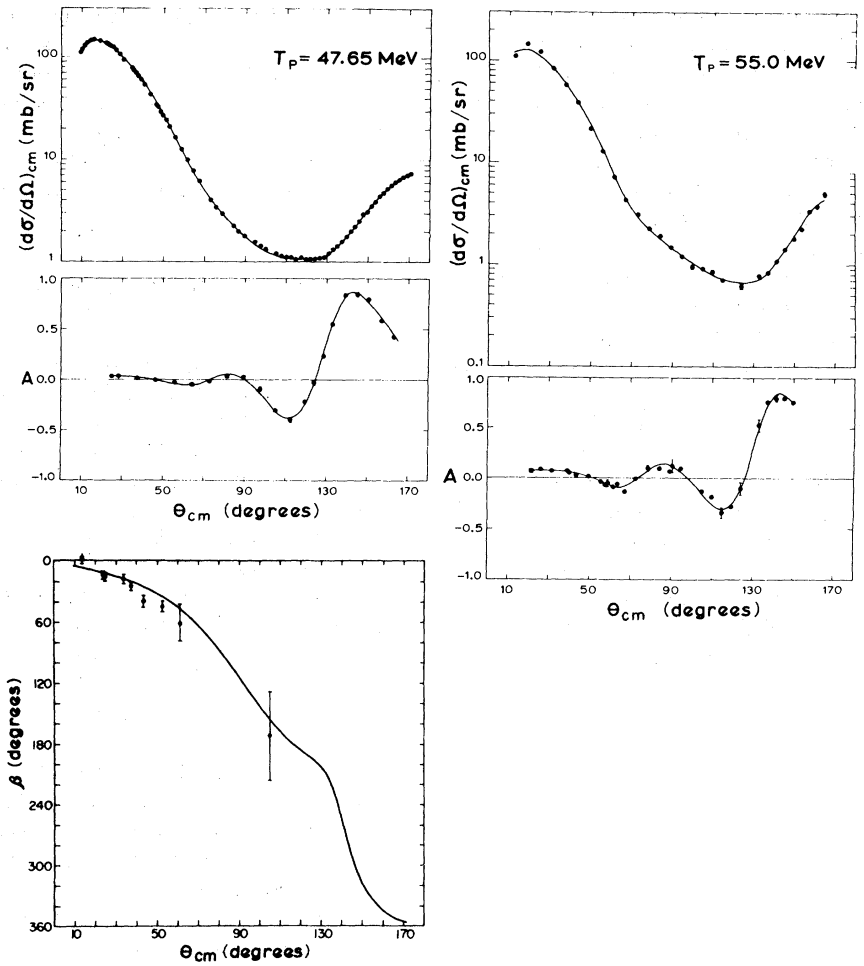

FIG. 6. Differential cross sections measured in the present experiment (47.65 MeV) and of Hayakawa *et al.* (55.0 MeV) analyzing powers of Craddock *et al.* (47.7 MeV) and of Boschitz *et al.* (54.8 MeV) and spin rotation parameters β of Griffith *et al.* (Ref. 21) (48.0 MeV). The solid curves represent the results of the present phase shift analysis.

scattering chamber center. The maximum error in the relative beam integration was taken to be 0.5%. At 39.75 MeV, measurements of the differential cross sections were repeated a number of times to check on the reproducibility. From these measurements a reproducibility uncertainty of ±1.3% was deduced.

Almost inevitably there was some build up of contaminants (mainly air) inside the gas cell during data taking runs. In order to be able to subtract a possible contribution of protons elastically scattered from nitrogen or oxygen at the extreme forward angles (where the energy resolution of the scintillator detectors was not good enough to separate protons elastically scattered from helium from those elastically scattered from nitrogen or oxygen), a series of measurements was made with the helium in the gas cell replaced by air. Subsequent analysis of the data showed that the contribution from an air contaminant was negligibly small except at three of the higher energies where corrections to the extreme forward angles ($\Theta_{lab} < 20°$) amounted to at most 2%. Measurements with the gas cell evacuated verified that the system of antiscattering baffles effectively prevented scattering from the gas cell foil from reaching any of the eight detectors in the array.

DATA ANALYSIS AND REDUCTION

The data were analyzed in two steps. First differential cross sections were obtained and then several corrections were applied to these cross sections. The extraction of the elastic scattering yields was straightforward except at very forward angles ($\Theta_{lab} < 20°$) at some of the higher energies where there was a small contribution from contaminants and at extreme backward angles where

the background underlying the elastic peak was non-negligible. The statistical error in the yields included an estimate of the possible error in the background subtraction. The uncertainty in the subtraction of the contaminant yields was taken to be 20% of the correction. Similarly the uncertainty in the deadtime correction was taken to be 20% of the correction. The various contributions to the relative error in the cross sections are given in Table II, while those to the absolute scale of the measurements are given in Table III.

Three additional corrections were applied to the data in order to account for effects due to (i) multiple scattering in the target gas and the foil covering the gas cell window, (ii) loss of elastically scattered protons in the scintillation crystals due to nuclear reactions, (iii) finite geometry. Corrections for multiple Coulomb-scattering effects were estimated using the expression given by Chase and Cox[14] and were found to be negligibly small. The fraction of elastically scattered protons lost from the main peak in the spectra was interpolated using various published results of this quantity.[15] This fraction varied between 1.2% at 30 MeV and 3.1% at 50 MeV. Finally the finite geometry correction took into account the fact that the measurements were done with finite solid angles, a beam of finite size traversing the gas target, and a beam which, in first approximation, converges towards the target. The finite geometry correction factor of Kan[16] was adapted to the particular conditions of the present experiment. The maximum correction occurred at forward angles and was always less than 1%. The laboratory cross sections were converted into center-of-mass differential cross sections using relativistic kinematics.

TABLE IV. Data selection for the phase shift analysis.

$d\sigma/d\Omega$	A	σ_R
21.85 [a]	21.90 [b]	
23.90 [a]	23.98 [b]	24.00 [c]
25.75 [a]	25.82 [b]	25.70 [c]
28.10 [a]	28.13 [b]	28.00 [c]
30.35 [a]	30.43 [b]	30.20 [c]
32.15 [a]	32.17 [b]	32.25 [c]
34.25 [a]	34.30 [b]	34.10 [c]
36.90 [a]	36.93 [b]	37.00 [c]
39.75 [a]	39.80 [b]	39.60 [c]
42.45 [a]		42.30 [c]
44.05 [a]	44.1 [d]	44.70 [c]
44.95 [a]		Interpolated
47.65 [a]	47.7 [e]	47.90 [c]
48.8 [f]		Interpolated
55.0 [g]	54.8 [d]	53.0 [h]

[a] Present experiment.
[b] Reference 2.
[c] Reference 3.
[d] Reference 28.
[e] M. K. Craddock, R. C. Hanna, L. P. Robertson, and B. W. Davies, Phys. Lett. 5, 335 (1963).
[f] Reference 19.
[g] Reference 20.
[h] D. J. Cairns, T. C. Griffith, G. J. Lush, A. J. Meteringham, and R. H. Thomas, Nucl. Phys. 60, 369 (1964).

RESULTS AND COMPARISON WITH PREVIOUS MEASUREMENTS

In the energy range covered by the present experiment there exists, in addition to the data of Bacher *et al.*,[2] differential cross-section angular distributions at 20.62, 23.34, 26.08, and 27.68 MeV by Allison and Smythe,[17] at 25.0, 26.1, 27.1, 28.2, and 29.2 MeV by Plummer *et al.*,[18] and excitation functions at $\Theta_{lab}=82.3°$, 92.3°, 102.3°, and 112.3° for the energy range 22.5–45.9 MeV plus a complete angular distribution at 46 MeV by Bunker *et al.*[12] It should be noted that the angular distributions of Bacher *et al.* were normalized using the data of Bunker *et al.* A comparison of the data mentioned is given in terms of excitation functions at $\Theta_{lab}=17.5°$, 37.5°, 82.3°, and 100° (Figs. 1 and 2). The data of the present experiment exhibit a rather smooth variation as function of energy. Note that the excitation function at 17.5° passes through the region of Coulomb-nuclear interference. It is apparent that there are small but significant discrepancies with the data of Bacher *et al.* at 17.5°. There may also be some slight discrepancies at 37.5° and 82.3° especially in the energy range between 25 and 35 MeV. The agreement at 100° is excellent. The data of Plummer *et al.* show a somewhat irregular energy variation that is inconsistent with the results of the present experiment. There is reasonable agreement with the data of Allison and Smythe. There is also good agreement with the 82.3° excitation function of Bunker *et al.*, except around 30 MeV where their excitation function appears to be slightly lower. Also shown in the two figures are cross sections deduced from previously measured angular distributions at 48.8 (Ref. 19) and 55.0 MeV.[20] The latter data points appear to extrapolate reasonably from the results of the present experiment.

The differential cross-section angular distributions obtained in the present experiment at incident proton energies of 21.85, 23.90, 25.75, 28.10, 30.35, 32.15, 34.25, 36.90, 39.75, 42.45, 44.05, 44.95, and 47.65 MeV are shown in Figs. 3–6. Note that the relative errors of the individual data points are in general less than 2%. Larger errors are connected with the extreme forward data

TABLE V. Single-energy phase shift solutions and related quantities for $p+{}^4$He elastic scattering between 20 and 55 MeV.

	21.85 MeV	23.90 MeV		25.75 MeV		28.10 MeV		30.35 MeV	
	δ (deg)	δ (deg)	η	δ (deg)	η	δ deg)	η	δ (deg)	
$^2S_{1/2}$	88.64	87.98	0.993	86.00	0.988	84.40	0.970	83.23	0.933
$^2P_{3/2}$	89.26	87.46	0.987	82.82	0.986	80.80	0.965	79.36	0.956
$^2P_{1/2}$	51.36	50.47	0.998	47.61	0.999	46.72	0.981	44.87	0.948
$^2D_{5/2}$	6.55	8.14	0.999	8.50	0.977	11.21	0.968	12.54	0.887
$^2D_{3/2}$	5.73	5.06	0.757	5.29	0.781	6.62	0.723	6.70	0.693
$^2F_{7/2}$	1.96	3.31	1.000	4.05	1.000	4.81	0.994	6.32	0.982
$^2F_{5/2}$	1.48	2.68	0.999	3.21	1.000	4.02	1.000	5.22	1.000
$^2G_{9/2}$	0.37	0.39	1.000	0.71	0.999	0.83	1.000	1.31	1.000
$^2G_{7/2}$	0.34	0.69	1.000	1.19	0.992	1.12	0.965	0.99	0.974
σ_R(mb)		39.7		41.5		61.3		80.9	
χ^2_σ	0.72	0.61		0.89		0.54		0.75	
χ^2_A	0.67	0.63		0.88		0.65		0.81	
$\chi^2_{\sigma_R}$		1.05		1.49		0.07		1.48	
χ^2_{tot}	0.69	0.77		1.08		0.42		1.01	

	32.15 MeV		34.25 MeV		36.90 MeV		39.75 MeV		42.45 MeV	
	δ (deg)	η	δ (deg)	η	δ (deg)	η	δ (deg)	η	δ (deg)	η
$^2S_{1/2}$	81.01	0.908	79.12	0.895	75.98	0.845	74.12	0.804	70.88	0.785
$^2P_{3/2}$	77.75	0.960	74.60	0.960	71.79	0.953	69.01	0.932	66.76	0.914
$^2P_{1/2}$	42.83	0.955	41.46	0.971	38.55	0.985	36.62	0.992	35.24	0.996
$^2D_{5/2}$	14.03	0.844	14.81	0.823	16.44	0.795	17.53	0.769	18.43	0.741
$^2D_{3/2}$	6.56	0.692	8.53	0.668	9 49	0.668	10.77	0.652	11.61	0.648
$^2F_{7/2}$	7.57	0.967	9.21	0.963	10.93	0.945	12.14	0.927	13.27	0.912
$^2F_{5/2}$	6.06	0.989	7.18	0.987	8.08	0.973	8.64	0.957	8.31	0.941
$^2G_{9/2}$	1.62	1.000	1.54	0.998	1.97	0.996	2.11	0.994	1.98	0.992
$^2G_{7/2}$	0.92	0.975	0.91	0.971	0.77	0.965	0.62	0.963	0.42	0.957
σ_R(mb)	89.0		91.6		99.0		106.4		111.2	
χ^2_σ	1.11		1.06		1.63		1.34		0.91	
χ^2_A	1.13		0.77		1.25		1.50		...	
$\chi^2_{\sigma_R}$	4.30		2.70		0.75		0.06		1.51	
χ^2_{tot}	2.17		1.51		1.20		0.96		1.20	

TABLE V. *(Continued)*.

	44.05 MeV		44.95 MeV		47.65 MeV		48.8 MeV		55 MeV	
	δ (deg)	η	δ (deg)	η	δ (deg)	η	δ (deg)	η	δ (deg)	η
$^2S_{1/2}$	71.64	0.770	69.96	0.772	68.88	0.761	70.83	0.761	64.61	0.763
$^2P_{3/3}$	65.28	0.908	65.37	0.904	63.42	0.895	63.07	0.892	61.39	0.882
$^2P_{1/2}$	34.03	0.998	34.61	0.998	33.23	0.997	33.31	0.998	32.86	0.997
$^2D_{5/2}$	19.49	0.731	19.91	0.720	21.00	0.704	22.45	0.700	24.44	0.693
$^2D_{3/2}$	12.00	0.643	12.40	0.646	12.78	0.650	13.82	0.636	11.92	0.657
$^2F_{7/2}$	13.82	0.903	13.91	0.898	14.29	0.876	15.10	0.875	14.85	0.871
$^2F_{5/2}$	7.81	0.934	8.07	0.925	7.78	0.914	6.98	0.905	6.23	0.879
$^2G_{9/2}$	1.77	0.898	1.70	0.987	1.45	0.980	1.32	0.978	1.23	0.959
$^2G_{7/2}$	0.32	0.955	0.25	0.954	0.21	0.953	0.05	0.948	−0.59	0.934
$^2H_{11/2}$	...	...	...	...	0.012	0.998	0.003	1.000	0.079	0.995
$^2H_{9/2}$	...	...	...	...	0.15	0.997	0.00	0.995	−0.132	0.994
σ_R(mb)	113.0		114.5		117.6		117.3		114.8	
χ^2_σ	1.07		0.92		1.03		1.66		1.99	
χ^2_A	1.80		...		1.29		...		0.81	
$\chi^2_{\sigma_R}$	1.86		2.21		1.23		0.44		0.001	
χ^2_{tot}	1.61		1.56		1.18		1.13		0.93	

points $10° < \Theta_{cm} < 20°$. The error in the absolute scale of the measurements is less than 2.5% (see Table III). The angular distributions show a smooth variation with energy as is also indicated by the excitation functions of Figs. 1 and 2. The data points of the present experiment in these figures were extracted by interpolation from the measured angular distributions. Numerical values of the differential cross section data can be obtained as an addendum to this paper from the authors.

DISCUSSION

The phase shift searches were performed with a modified version of the program PEGGY.[22] The modifications made it possible to fit differential cross section and analyzing power data at different sets of angles and to enter the total reaction cross section as an additional datum. The modified program also calculated the spin rotation parameter β. The searches were performed by

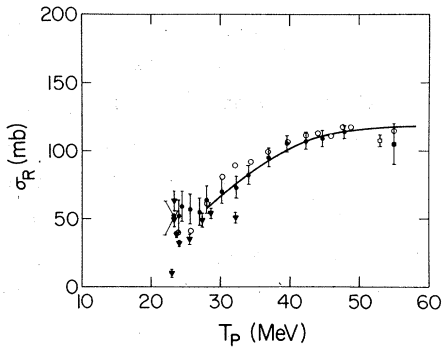

FIG. 7. The $p + {}^4$He total reaction cross section from threshold (23.02 MeV) to 55 MeV. The open circles represent the results of the present single energy phase shift solutions. The filled triangles give values deduced by applying detailed balance to the results of measurements (Refs. 23 and 24) on the reaction $d + {}^3$He $\rightarrow p + {}^4$He. The other experimental data are from Sourkes *et al.*, Hayakawa *et al.*, and Cairns *et al.* The solid line is the total reaction cross section calculated using the resonating-group method (Ref. 3).

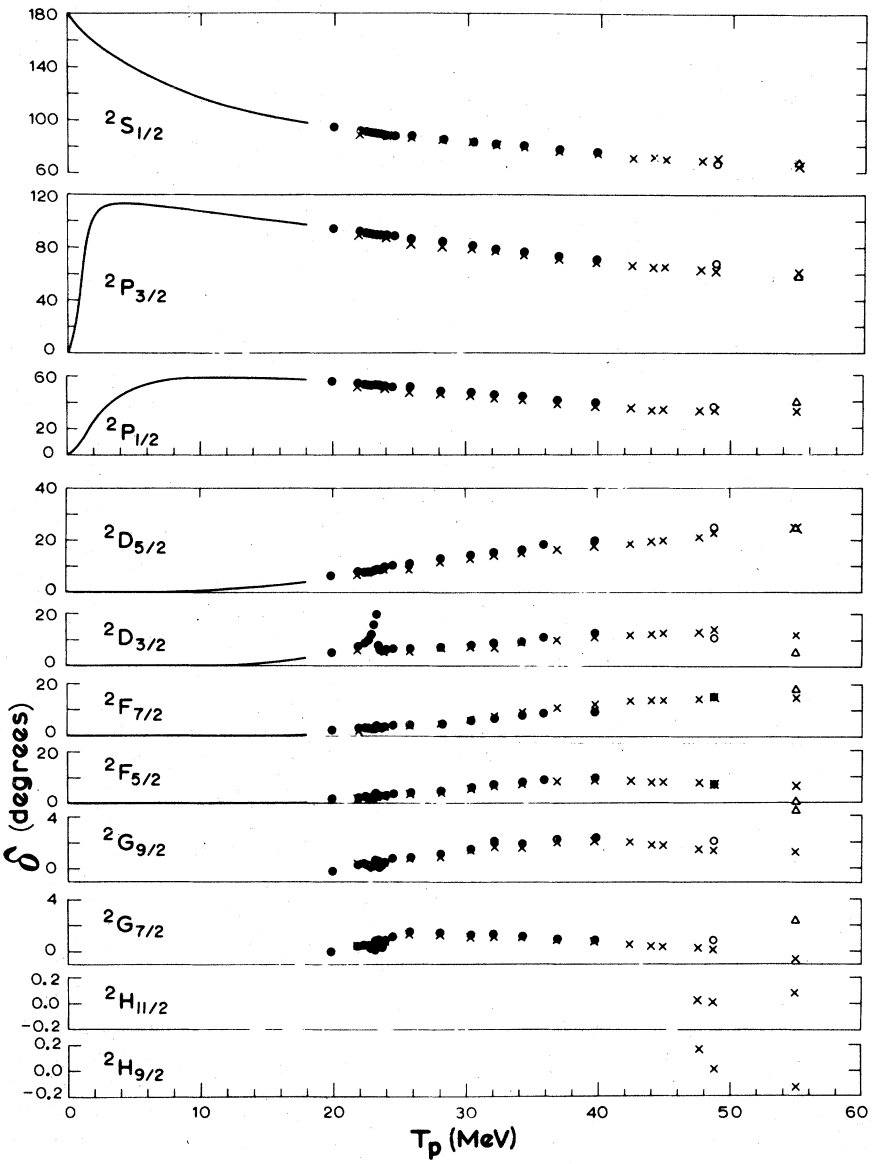

FIG. 8. Real parts of the S-, P-, D-, F-, G-, and H-wave phase shifts for $p+{}^4$He elastic scattering. The crosses give the results of the present analysis. The solid lines below 18 MeV represent the energy-dependent phase shift solution of Schwandt *et al.* The solid dots indicate the results of the phase shift analysis of Plattner *et al.* while the symbol 0 at 48.8 MeV is taken from the phase shift analysis of Davies *et al.* and the symbol Δ at 55.0 MeV from the phase shift analysis of Horikawa *et al.*

minimizing the quantity χ^2 defined as

$$\chi^2 = \frac{A}{N_\sigma}\sum_{i=1}^{N_\sigma}\left(\frac{\sigma^{\rm th}(\Theta_i)-\sigma^{\rm exp}(\Theta_i)}{\Delta\sigma(\Theta_i)}\right)^2 + \frac{B}{N_A}\sum_{j=1}^{N_A}\left(\frac{A^{\rm th}(\Theta_j)-A^{\rm exp}(\Theta_j)}{\Delta A(\Theta_j)}\right)^2 + C\left(\frac{\sigma_R^{\rm th}-\sigma_R^{\rm exp}}{\Delta\sigma_R}\right)^2,$$

where $\sigma^{\rm th}(\Theta_i)$ and $\sigma^{\rm exp}(\Theta_i)$ are calculated and experimental differential cross sections at the N_σ center-of-mass scattering angles Θ_i; $A^{\rm th}(\Theta_j)$ and $A^{\rm exp}(\Theta_j)$ are the calculated and experimental analyzing powers at the N_A center-of-mass scattering angles Θ_j; $\sigma_R^{\rm th}$ and $\sigma_R^{\rm exp}$ are the calculated and experimental total reaction cross sections; and $\Delta\sigma(\Theta_i)$, $\Delta A(\Theta_j)$, and $\Delta\sigma_R$ are the corresponding experimental errors. The quantities A, B, and C are weighting factors which were usually set equal to 9, 5, and 1 to enhance the sensitivity with respect to the analyzing power data and the reaction cross-section datum. Other combinations

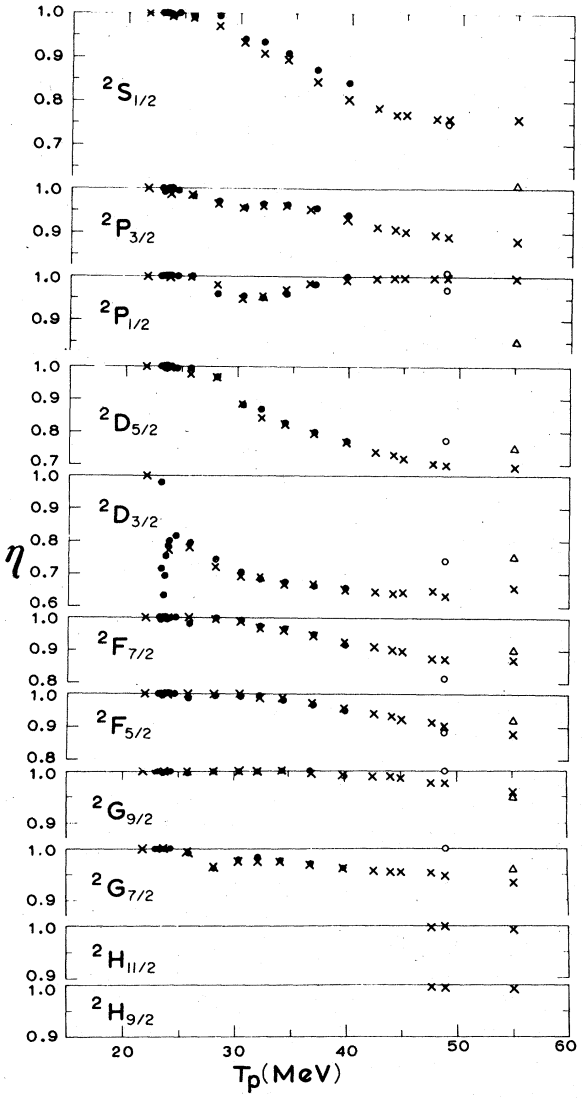

FIG. 9. Absorption parameters of the S-, P-, D-, F-, G-, and H-wave phase shifts for $p+{}^4$He elastic scattering. The crosses give the results of the present analysis. The solid dots indicate the results of the phase shift analysis of Plattner *et al.* while the symbol 0 at 48.8 MeV is taken from the phase shift analysis of Davies *et al.* and the symbol Δ at 55.0 MeV from the phase shift analysis of Horikawa *et al.*

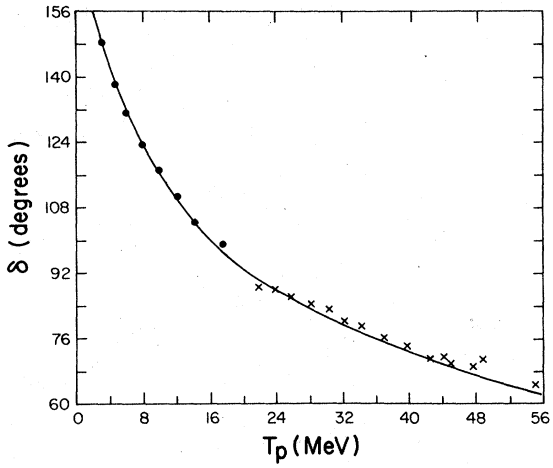

FIG. 10. The $^2S_{1/2}$ wave phase shifts as function of incident proton energy. The present single energy phase shift solutions between 20 and 55 MeV are given by the crosses. The dots indicate the $^2S_{1/2}$ wave phase shifts obtained by Schwandt *et al.* The solid curve represents an effective range expansion fit to the S-wave shift as mentioned in the text.

of weighting factors were also tried, leading to essentially the same final result.

The experimental information on differential cross sections, analyzing powers, and total reaction cross sections selected for the phase shift analysis is indicated in Table IV. The decision not to use other experimental information, i.e., other differential cross-section data, was based upon the comparisons of existing data presented above. Unfortunately, some of the higher energy experimental data from the literature, included in the phase shift analysis, have uncertainties considerably larger than the experimental errors of the present experiment or those of Bacher *et al.*[2] and Sourkes *et al.*[3]

Since in the energy range of interest, that is above 20 MeV, the phase shifts should behave as rather smooth functions of energy (with the exception of the $^2D_{3/2}$ phase shift), the search at a particular energy was initiated with guess values set equal to the solution at the next lower energy. In addition, searches were also started with guess values obtained by interpolation or extrapolation from the solutions of Plattner et al.[1] At a number of energies much larger variations in the starting values for the phase shift searches were also tried, but in all cases the searches converged to nearly the same solution. The procedure followed yielded satisfactory fits with 18 parameters (complex S-, P-, D-, F-, and G-wave phase shifts) at energies between 23 and 45 MeV and 22 parameters (complex S-, P-, D-, F-, G-, and H-wave phase shifts) at energies above 45 Mev. At 21.85 MeV the fit was obtained with nine parameters (real S-, P-, D-, F-, and G-wave phase shifts). Inclusion of the $^2H_{9/2}$ and $^2H_{11/2}$ waves at 47.65, 48.8, and 55.0 MeV significantly improved the fits to the experimental data reducing for instance the value of χ^2_{tot} at 47.65 MeV from 1.50 to 1.18. The final results of the phase shift analysis are presented in Table V. Also given in Table V are the χ^2 values per data point for the differential cross sections, the analyzing powers, and the total

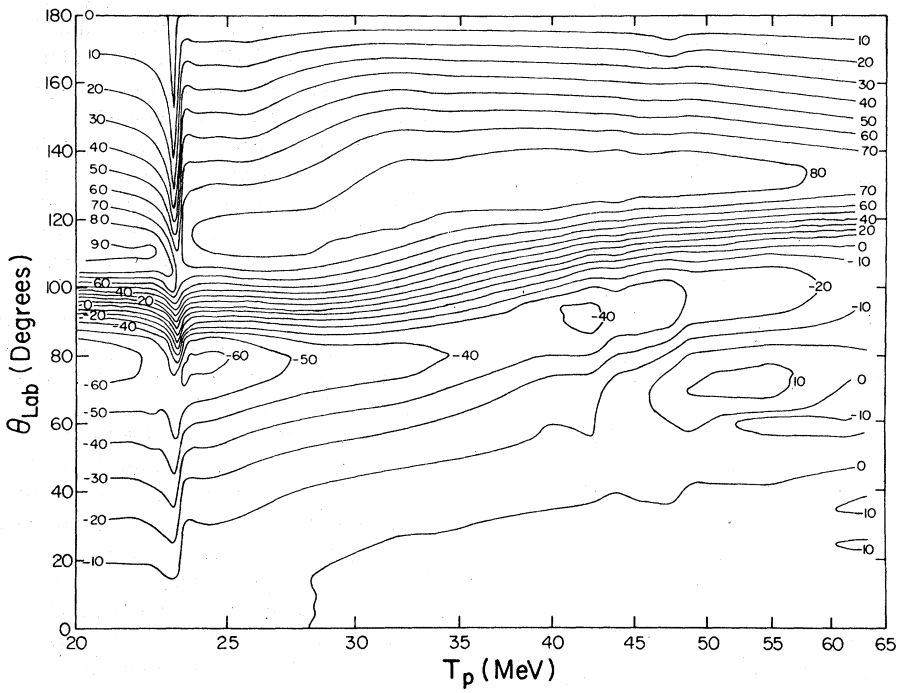

FIG. 11. Analyzing power contour diagram for $p+{}^4$He elastic scattering between 20 and 65 MeV based on the phase shift analysis of Plattner *et al.* (Ref. 1), on the present phase shift analysis and on the data of Boschitz *et al.*

reaction cross sections separately, as well as χ^2_{tot} which (to facilitate comparisons) is defined as the average of the three individual χ^2 values (χ^2_{tot} is the value of χ^2 defined above divided by the quantity $A+B+C$). Also entered in Table V are the calculated values for the total reaction cross section.

The sensitivity of the fits with regard to variations of the individual phase shifts was tested at 25.75 and 39.75 MeV. The χ^2_{tot} variation was studied for each individual phase shift keeping the values of all other phase shifts equal to those corresponding to the accepted solution given in Table V. For instance, at 39.75 MeV a change in χ^2_{tot} from a value of 0.96 to a value of 1.96 corresponds to $\Delta\delta(^2S_{1/2}) = +0.86°$, $-1.13°$; $\Delta\delta(^2P_{3/2}) = +0.81°$, $-0.67°$; $\Delta\delta(^2P_{1/2}) = +0.79°$, $-0.69°$; $\Delta\delta(^2D_{5/2}) = +0.37°$, $-0.50°$; $\Delta\delta(^2D_{3/2}) = +0.66°$, $-0.71°$; and $\Delta\eta(^2S_{1/2}) = +0.018$, -0.014; $\Delta\eta(^2P_{3/2}) = +0.016$, -0.017; $\Delta\eta(^2P_{1/2}) = -0.019$; $\Delta\eta(^2D_{5/2}) = +0.019$, -0.019; $\Delta\eta(^2D_{3/2}) = +0.022$, -0.021. Similar results were obtained at 25.75 MeV.

The fits to the experimental data are shown in Figs. 3–6 as solid lines. It is apparent that the quality of the fits is excellent at all energies. A comparison between the total reaction cross sections, calculated from the inelastic parameters, and the experimental data is shown in Fig. 7. Again the good agreement is apparent. It should be remarked that in general the sensitivity of σ_R with regard to variations of the individual inelastic parameters is less than the sensitivity of χ^2_{tot} with regard to variations in either the real parts or the imaginary parts of the phase shifts.

The p-^{4}He phase shifts are shown in Figs. 8 and 9 as a function of energy between 0 and 55 MeV. The solid lines below 18 MeV represent the results of the energy-dependent phase shift solution of Schwandt *et al.*[5] Also indicated are the results of the phase shift analysis of Plattner *et al.*,[1] of Davies *et al.*,[19] and of Horikawa *et al.*[25] It is clear that the phase shifts show a rather continuous behavior from 0 to 55 MeV supporting the assumption that the results shown form a good approximation to the correct set of phase shifts. The following observations can be made:

(1) Both the real and imaginary parts of the $^2S_{1/2}$ phase shifts are systematically somewhat smaller than those of Plattner *et al.*[1] at the corresponding energies. Figure 10 shows the $^2S_{1/2}$ phase shifts as a function of incident proton energy. The present single energy phase shift solutions between 20 and 55 MeV are given by the crosses while the dots indicate the $^2S_{1/2}$ wave phase shifts obtained by Schwandt *et al.*[5] The solid curve represents an effective range expansion type fit to the $^2S_{1/2}$-wave phase shifts, $\delta = a + bT$ with parameters $a = 106$ and $b = -0.776$ Mev^{-1}, showing excellent continuity.

(2) Absorption takes place primarily in the even

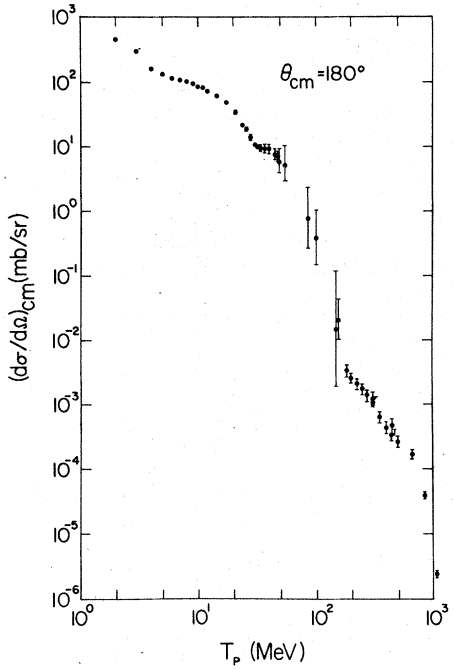

FIG. 12. Excitation function for ^{4}He(p,p) elastic scattering at $\theta_{c.m.}$ = 180° in the energy range 1 MeV to 1 GeV. Below 20 MeV the data points were obtained by extrapolating the angular distributions of Barnard *et al.* (Ref. 29), Hutson *et al.* (Ref. 30), and Garreta *et al.* (Ref. 31). Above 55 MeV the data points were obtained by extrapolating the angular distributions of Votta *et al.* (Ref. 32), Goldstein *et al.* (Ref. 33), Cormack *et al.* (Ref. 34), Comparat *et al.* (Ref. 35), Berger *et al.* (Ref. 36), and Cameron *et al.* (Ref. 37). Between 20 and 55 MeV the data points were obtained from the phase shift fits to angular distributions listed in Table IV.

partial waves, in particular in the $^2D_{3/2}$ and $^2D_{5/2}$ partial waves. However, just above threshold in the region of the $^2D_{3/2}$ resonance the inelasticity is practically confined to that particular partial wave as shown in the phase shift analysis of Plattner *et al.*[1]

(3) Both the $^2P_{3/2}$ and $^2P_{1/2}$ inelastic parameters exhibit a somewhat anomalous behavior around an incident proton energy of 30 MeV. The absorption first increases and then decreases to stay rather constant at energies above 40 MeV. Evidence for broad and overlapping resonant states with $J^\pi = \frac{1}{2}^-$ and $\frac{3}{2}^-$ have come from analyses of the reactions ^{3}He(d,p)^{4}He, ^{3}He(d,d)^{3}He, ^{3}H(d,d)^{3}H, and ^{3}He($d,2p$)^{3}H and ^{3}H(d,pn)^{3}H.[26] It should be noted that there is very little splitting of the real parts of the F-wave phase shifts up to 40 MeV.

(4) The G waves are important over the whole energy range 20–55 MeV and are necessary to fit the detailed shape of the differential cross section angular distributions.

(5) There is some indication (from the $^2G_{7/2}$ phase shifts) of a $\frac{7}{2}^+$ level around 29 MeV also deduced by Seiler[26] from an analysis of the ^{3}He($\vec{d}$, p)^{4}He reaction and furthermore appearing in the extension of the R-matrix analysis of the mass-5 system by Dodder and Hale.[27]

(6) Above 40 MeV the phase shifts continue a smooth behavior as function of energy. There is good agreement between the real parts of the phase shifts obtained in the analysis of Davies *et al.*[19] and those of the present work but less so between the two sets of inelastic parameters. The agreement between the phase shifts deduced by Horikawa *et al.*[25] at 55 MeV and those of the present work is poor.

As shown in Fig. 11, ^{4}He is an excellent polarization analyzer. The contour diagram shown is constructed from the phase shift solutions of Plattner *et al.*[1] up to and including the resonance region, from the phase shift solutions of the present work at higher energies, and from an additional analyzing power angular distribution at 63.3 MeV from Boschitz *et al.*[28] Except for the strong anomaly around 23.4 MeV, corresponding to the $^2D_{3/2}$ resonance in ^{5}Li, the contour lines show little angular variation from 25 MeV onward up to 60 MeV especially in the backward hemisphere although one may remark a slight change around 30 MeV. In the forward hemisphere there are some pronounced changes which occur at energies above 60 MeV. In the energy region 30–60 MeV, the polarizations between 125° and 140° cm are larger than 0.8, although the maximum decreases slowly with energy.

The p + ^{4}He differential cross section angular distributions are backward peaked for incident proton energies up to 150 MeV. At energies above 150 MeV the simple three-nucleon exhange mechanism, important at low energies, appears to be overshadowed by other exchange processes and the differential cross section angular distributions become flat for extreme backward angles. At still higher energies backward peaking of the angular distributions reappears. Based upon a linear extropolation of the logarithmic value of the differential cross sections versus the cosine of the scattering angle, a 180° excitation function was constructed and exhibited in Fig. 12. Three marked shoulders appear to exist in the excitation function. The second one near 40 MeV is due to the particular interplay of the P- and D-wave phase shifts. The third one between approximately 200 and 600 MeV is probably related to more complicated exchange processes although it should be remarked that the momentum transfers involved at these energies correspond to the region of the second maximum in the ^{4}He form factor.[38]

*Work supported in part by the Atomic Energy Control Board of Canada.

†Present address: Department of Physics, University of Riyadh, Riyadh, Saudi Arabia.

‡Present address: Manitoba Cancer Treatment and Research Foundation, Winnipeg, Manitoba.

[1]G. R. Plattner, A. D. Bacher, and H. E. Conzett, Phys. Rev. C 5, 1158 (1972).

[2]A. D. Bacher, G. R. Plattner, H. E. Conzett, D. J. Clark, H. Grunder, and W. F. Tivol, Phys. Rev. C 5, 1147 (1972).

[3]A. M. Sourkes, N. E. Davison, S. A. Elbakr, J. L. Horton, A. Houdayer, W. T. H. van Oers, and R. F. Carlson, Phys. Lett. 51B, 232 (1974); A. M. Sourkes, A. Houdayer, W. T. H. van Oers, R. F. Carlson, and R. E. Brown, Phys. Rev. C 13, 451 (1976).

[4]G. R. Satchler, L. W. Owen, A. J. Elwyn, G. L. Morgan, and R. L. Walter, Nucl. Phys. A112, 1 (1968).

[5]P. Schwandt, T. B. Clegg, and W. Haeberli, Nucl. Phys. A163, 432 (1971).

[6]R. A. Arndt, L. D. Roper, and R. L. Shotwell, Phys. Rev. C 3, 2100 (1971).

[7]Th. Stammbach and R. L. Walter, Nucl. Phys. A180, 225 (1972).

[8]D. C. Dodder, G. M. Hale, N. Jarmie, J. H. Jett, P. W. Keaton, Jr., R. A. Nisley, and K. Witte, Phys. Rev. C 15, 518 (1977).

[9]M. E. Brandan, G. R. Plattner, and W. Haeberli, Nucl. Phys. A263, 189 (1976).

[10]B. M. Bardin and M. E. Rickey, Rev. Sci. Instrum. 35, 902 (1964); R. Smythe, *ibid.* 35, 1197 (1964).

[11]P. Darriulat, D. Garreta, A. Tarrats, and J. Testoni, Nucl. Phys. A108, 316 (1968).

[12]S. N. Bunker, J. M. Cameron, M. B. Epstein, G. Paić, J. R. Richardson, J. G. Rogers, P. Tomaš, and J. W. Verba, Nucl. Phys. A133, 537 (1969).

[13]E. A. Silverstein, Nucl. Instrum. 4, 53 (1959).

[14]C. T. Chase and R. T. Cox, Phys. Rev. 58, 243 (1940).

[15]L. H. Johnston, D. F. Service, and D. A. Swenson, Trans. I. R. E. NS-5, 95 (1958); D. F. Measday and C. Richard-Serre, Nucl. Instrum. 76, 45 (1969).

[16]J. T. C. Kan, Rev. Sci. Instrum. 44, 323 (1973).

[17]P. W. Allison and R. Smythe, Nucl. Phys. A121, 97 (1968).

[18]D. J. Plummer, K. Ramavataram, T. A. Hodges, D. G. Montague, A. Zucker, and N. K. Ganguly, Nucl. Phys. A174, 193 (1971).

[19]B. W. Davies, M. K. Craddock, R. C. Hanna, Z. J. Moroz, and L. P. Robertson, Nucl. Phys. A97, 241 (1967).

[20]S. Hayakawa, N. Horikawa, R. Kajikawa, K. Kikuchi, H. Kobayakawa, K. Matsuda, S. Nagata, and Y. Sumi, J. Phys. Soc. Jpn. 19, 2004 (1964).

[21]T. C. Griffith, D. C. Imrie, G. J. Lush, and L. A. Robbins, Phys. Rev. 146, 626 (1966).

[22]L. W. Owen, Oak Ridge National Laboratory Report No. ORNL-TM-1464 (unpublished).

[23]J. L. Yarnell, R. H. Lovberg, and W. R. Stratton, Phys. Rev. 90, 292 (1953).

[24]T. W. Bonner, J. P. Conner, and A. B. Lillie, Phys. Rev. 88, 473 (1952); A. P. Kliucharev, B. N. Esel'son, and A. K. Val'ter, Dokl. Akad. Nauk. SSSR 109, 737 (1956) [Sov. Phys.-Dokl. 1, 475 (1956)]; L. Stewart, J. E. Brolley, Jr., and L. Rosen, Phys. Rev. 119, 1649 (1960); T. R. King and R. Smythe, Nucl. Phys. A183, 657 (1972).

[25]N. Horikawa and H. Kanada, J. Phys. Soc. Jpn. 20, 1758 (1965).

[26]F. Seiler, Nucl. Phys. A244, 236 (1975).

[27]D. C. Dodder and G. M. Hale, private communication.

[28]E. T. Boschitz, M. Chabre, H. E. Conzett, H. E. Shield, and R. J. Slobodrian, in *Proceedings of the Second International Symposium on Polarization Phenomena of Nucleons* (Birkhauser, Basel, 1966), p. 328.

[29]A. C. L. Barnard, C. M. Jones, and J. L. Weil, Nucl. Phys. 50, 604 (1964).

[30]R.L. Hutson, N. Jarmie, J. L. Detch, Jr., and J. H. Jett, Phys. Rev. C 4, 17 (1971).

[31]D. Garreta, J. Sura, and A. Tarrats, Nucl. Phys. A132, 204 (1969).

[32]L. G. Votta, P. G. Roos, N. S. Chant, and R. Woody, III, Phys. Rev. C 10, 520 (1974).

[33]N. P. Goldstein, A. Held, and D. G. Stairs, Can. J. Phys. 48, 2629 (1970).

[34]A. M. Cormack, J. N. Palmieri, N. F. Ramsey, and R. Wilson, Phys. Rev. 115, 599 (1959).

[35]V. Comparat, R. Frascaria, N. Fujiwara, N. Marty, M. Morlet, P. G. Roos, and A. Willis, Phys. Rev. C 12, 251 (1975).

[36]J. Berger, J. Duflo, L. Goldzahl, F. Plouin, J. Oostens, M. van den Bossche, L. Vu Hai, G. Bizard, C. Le Brun, F. L. Fabbri, P. Picozza, and L. Satta, Phys. Lett. 63B, 111 (1976); and contribution to the VII International Conference on High Energy Physics and Nuclear Structure, Zürich, 1977 (unpublished).

[37]J. M. Cameron, L. G. Greeniaus, D. A. Hutcheon, R. H. McCamis, C. A. Miller, G. A. Moss, G. Roy, M. S. de Jong, B. T. Murdoch, W. T. H. van Oers, J. G. Rogers, and A. W. Stetz, contribution to the VII International Conference on High Energy Physics and Nuclear Structure, Zürich, 1977 (unpublished).

[38]H. Leśniak, L. Leśniak, and T. Tekou, Nucl. Phys. A267, 503 (1976).